A study of fracture behaviour of gamma lamella using the notched TiAl micro-cantilever

Ding, Rengen; Chiu, Yu-Lung; Chu, Mingqiang; Paddea, Sanjooram; Su, Guangqiao

DOI:
10.1080/14786435.2020.1714088

Document Version
Peer reviewed version

Citation for published version (Harvard):
Ding, R, Chiu, Y-L, Chu, M, Paddea, S & Su, G 2020, 'A study of fracture behaviour of gamma lamella using the notched TiAl micro-cantilever', *Philosophical Magazine*, vol. 100, no. 8, pp. 982-997. https://doi.org/10.1080/14786435.2020.1714088

A study of fracture behaviour of gamma lamella using the notched TiAl micro-cantilever

Rengen Ding[1, 2], Yulung Chiu[1], Mingqiang Chu[2], Sanjooram Paddea[3], and Guanqiao Su[4]

1. School of Metallurgy and Materials, University of Birmingham, Edgbaston, Birmingham, B15 2TT, UK
2. Centre of Excellence for Advanced Materials, No.1 Libin Road, Songshan Lake, Dongguan, Guangdong, China
3. International Stress Centre, Open University, Milton Keynes, MK7 6AA, UK
4. State Key Laboratory of Rolling and Automation, Northeastern University, Shenyang 110819, China

Abstract

Microcantilevers were machined from a single γ(TiAl)-α_2(Ti_3Al) lamellae colony of a polycrystalline commercial Ti-45Al-2Mn-2Nb sample using the focussed ion beam. The long axis of the microcantilevers is perpendicular to the lamellar interface with the notch prepared in the same γ lamella. Bending test results demonstrated good repeatability and the fracture stress intensity factor of individual γ lamella was measured to be 3.1 ± 0.2 MPa $m^{1/2}$. $(\bar{1}\bar{1}1)[\bar{1}\bar{1}\bar{2}]$ twinning ahead of the notch (crack) tip plays a key role in the crack initiation. TEM analysis shows that the interaction of twinning with the lamellar interface leads to interfacial cracking and contributes to the work-hardening observed.

Introduction

γ-TiAl alloys with fully lamellar microstructure, consisting predominantly of parallel γ (TiAl) and fewer α_2 (Ti_3Al) lamellae, generates a good balance of tensile, fatigue and creep properties and is often desirable for many applications [1, 2]. Due to their different crystal structures, the γ and α_2 phases show distinct deformation behaviours. As a consequence, these two phases experience different plastic deformations even under the same macroscopically homogeneous straining condition. Even for γ lamellae, however, there are three types of γ/γ interfaces that are termed either pseudo-twins (PT, 60°), order variants (OV, 120°) or true twins (TT, 180°). Although the transmission of unit dislocations ($\{111\}\frac{1}{2}<110]_\gamma$) and twinning ($\{111\}\frac{1}{2}<11\bar{2}]_\gamma$) through the γ/γ interface is relatively easier than through the γ/α_2 interface [3], both γ/γ and γ/α_2 interfaces can act as barriers to dislocation slip and twinning. Thus, examination of the 'global' mechanical properties only is insufficient to depict the deformation behaviour of such lamellar alloy. Investigation on local deformation behaviour of individual lamella is necessary to achieve deeper insights into deformation

mechanisms. Recently, microscale mechanical testing (e.g. compression and tension) of lamellar γ-TiAl alloys has been reported [4-7]. Rester et al. [5] have found that twinning width increases with γ lamella thickness. Palomares-García et al. [4] have studied that the influence of lamellar orientations on the strength and operative deformation mechanisms of a fully lamellar Ti-45Al-2Nb-2Mn (at.%)+ 0.8(vol.%) TiB_2 alloy, and found that the mechanical response of the alloy is controlled by the interaction of twin/slip with the lamellar interface. Edwards et al. [7, 8] have also demonstrated that the longitudinal twinning (where twin shear // the interfacial planes) is a main deformation mechanism in soft-orienation pillars (where the angle between lamellae and pillar axis is 30-60°). These investigations have revealed that the mechanical behaviours are governed by deformation modes, e.g. longitudinal (i.e., 'soft') and transverse (i.e., 'hard') modes. However, those mechanical responses recorded still came from several lamellae not from an individual lamella. In other words, those mechanical behaviours are affected somewhat by lamellar interfaces. The mechanical property (e.g. fracture toughness) of an individual lamella is desirable because that not only provides the input for modelling but also is crucial to further understand the role of lamella interface via comparison to the property obtained from the mulitple lamellae.

It has been demonstrated that the notched microcantilever test is a reliable method to evaluate fracture properties of 'brittle' materials or materials with limited plasticity. For instance, Iqbal et al. [9] have used in-situ microcantilever test to study the influence of orientation on the fracture toughness of NiAl single crystals. Chan et al. have investigated fracture properties of micro-scale zirconium hydrides and phase boundaries via microcantilever testing methods [10]. Deng and Barnoush have used the notched microcantilever test to study the effect of hydrogen on fracture behaviours of FeAl intermetallic [11]. Halford et al. [12] have carried out ex-situ microcantilever tests on lamellar TiAl alloys to measure the fracture toughness and found that the fracture toughness at the micro-scale is lower than that of the corresponding bulk sample although the data scatter is relatively large. It should be noted here that the notches did not have the same relationship with respect to lamellar interfaces.

The aim of this paper is to measure the fracture toughness of the individual γ phase and to understand its failure behaviour. To do this, the notch for all microcantilevers was fabricated in the same γ lamella. Deformation substructure (in particular, twin) was analysed using transmission electron microscopy (TEM), and fracture surfaces of the failed microcantilevers were examined in a scanning electron microscope (SEM).

2. Experimental procedures

2.1 Material and preparation

A commercial Ti-45Al-2Mn-2Nb (at.%) (Ti4522) alloy was used in this study. This system was chosen because it is one of the most promising γ-TiAl alloys for low pressure turbine blade application [13]. The sample surface was ground and mechanically polished, followed by electrochemical polishing at a voltage of 25 V in a solution of 5% perchloric acid, 35% butanol and 60% methanol. A large colony with ~2 mm diameter was selected via electron backscatter diffraction (EBSD) such that the normal of the sample surface is parallel to the interfaces with a small deviation of 5°.

2.2 Microcantilever fabrication and testing

Cantilevers with pentagonal cross-section were fabricated using a FEI Quant 3D Dual-Beam FIB system, with an acceleration voltage of 30kV. Higher ion beam currents of 7 to 15 nA were used for the first coarse milling. The final cleaning steps were performed using a 100 pA to minimize the Ga ion beam damaging effect. A single line pass with a low ion current (10 pA) was used to mill a notch. The notch was ~1.0 μm away from the built-in end of the microcantilever. This low beam current produced a sharp notch tip with a diameter ~10 nm (which is measured using TEM image). The notches for all microcantilevers were milled in the same γ lamella, as shown in Fig. 1a. The size of a representative microcantilever is illustrated in Fig. 1b. The finished microcantilever was ~ 15 μm long, where the length between the notch and the loading point L was 12 μm, with a pentagonal cross-section and a notch depth of 0.2~0.75 μm. A fiducial mark of 500 nm depth and 500 nm diameter was made to achieve a well-defined loading point.

The microcantilevers were tested in-situ using a Hysitron PI85 picoindenter mounted inside a Tescan Mira-3 SEM using a Berkovich tip under displacement-controlled mode with the displacement rate of 1 nm/s. The deformed microcantilevers were examined using SEM.

2.3 Stress intensity factor

Load-deflection curves were evaluated using linear elastic fracture mechanics (LEFM). The plane strain stress intensity factor assuming mode I loading K_I was calculated, as in other micromechanical fracture work [10, 11, 14, 15].

$$K_I = \sigma\sqrt{\pi a}F\left(\frac{a}{2\bar{y}}\right) \quad (1)$$

$$\sigma = \frac{PL\bar{y}}{I} \quad (2)$$

Where a is the notch depth and $\bar{y}$ is the vertical distance between the upper surface and the centroid of the cross-section. P is the applied load, L is the distance between the notch and

the loading point and I is the second moment of area. $F(\frac{a}{2\bar{y}})$ is a dimensionless shape factor, which depends on the geometry of the sample. The two available factors for a pentagonal cross-section were computed numerically [10, 14]. The boundary-element method was adopted in ref. [14] while Chan et al. [10] used the finite element method with three-dimension quadratic elements. The solution of F in ref. [10] compares well with the F established from rectangular cross-sections [9, 15, 16] while the factor from ref. [14] is noticeably higher than the others. In this study the solution of Chan et al. [10] was adopted:

$$F\left(\frac{a}{2\bar{y}}\right) = 3.710\left(\frac{a}{2\bar{y}}\right)^3 - 0.630\left(\frac{a}{2\bar{y}}\right)^2 + 0.242\left(\frac{a}{2\bar{y}}\right) + 0.974$$

2.4 Microstructure

TEM was used to analyse microstructure of the deformed microcantilevers. TEM foils were prepared along the longitudinal direction of the microcantilevers by FIB. A Pt coating was used to protect the top surface of the deformed microcantilevers. The initial stages of foil preparation used a 30 keV ion beam with the probe current reduced successively throughout the procedure and a final polishing/cleaning was performed at 5kV. TEM examination was carried out in a FEI Talos F200X scanning transmission electron microscope (STEM) with a double-tilt specimen holder and an accelerating voltage of 200 kV. Upon examination of the TEM samples, it was found that bending of the foils caused a problem for conventional diffraction contrast imaging, especially when trying to image entire sections. Bright-field STEM imaging was used to minimize these effects, as in our previous studies of Ti-6Al-4V micro-cantilevers [17, 18].

3. Results and discussion

3.1 Mechanical loading

To examine the reliability of the current approach, microcantilevers with different notch depths were prepared and tested. Figure 2 exhibits some typical load-deflection curves, showing a good repeatability. Figure 2 also shows that the load at yield point decreases with increasing notch depth. However, stress intensity factor (K_I) for the microcantilevers does not clearly change with notch depth or notch position, as seen in Table 1. All these observations suggest that the notched cantilever test is reliable to evaluate fracture properties of an individual γ lamella. Figure 2 also indicates that all tests show an obviously positive slope beyond yielding (work-hardening), which is in good agreement with the literature, i.e., the highest work-hardening was observed when loading axis is perpendicular to lamellae [4].

Sudden load drops were observed (Fig. 2), which could be related to the activating of slip bands or twinning. For instance, after sudden load drops (arrowed in Fig. 2), slip traces/twinning (arrowed in Fig. 3) were observed on the top surface of the microcantilever. In order to explore the role of interface, the microcantilevers without notch or with the notch very close to the interface were prepared and tested. The microcantilever without the notch shows a similar load-deflection curve obtained from the microcantilever with a short notch depth (Fig. 4). However, the microcantilever with the notch close to the lamellar interface displays different behaviours such as a lower work-hardening. These interesting observations indicate that the fracture behaviour is probably correlated with the interaction of deformation microstructure with the interfaces. To explore this viewpoint, some microcantilevers were interrupted at the deflection of ~1.5 μm during bending, their deformation structures were analysed via TEM. The results will be presented in Section 3.2.

The stress intensity factor K_I derived is shown in Fig. 5 together with the literature data obtained using different test methods. The measured K_I value of the γ lamella in Ti4522 alloy is 3.1 ± 0.2 MPa $m^{1/2}$, which is much lower than the fracture toughness values reported in bulk γ-TiAl alloys, ~16-30 $MPam^{1/2}$ depending on the microstructure and composition [19, 20]. This discrepancy is because the bulk sample includes the contribution from grain boundaries and interfaces. The K_I obtained in the current work is in good agreement with the reported data [21-24] (Fig. 5), i.e., between Ti49Al and Ti51Al alloys using compact tension (CT) specimens [21] but higher than the microcantilever result obtained from Ti48Al (1.9 $MPam^{1/2}$) [22]. This is probably attributed to the composition difference. Here, it should be mentioned that Ga^+ ions notching could affect the toughness values measured. Best et al. [25] did a comparison of three different notching ions (i.e. Ga^+, Xe^+, and He^+) for small-scale fracture toughness measurement of CrN thin film, and found that the microcantilever notched using Ga^+ showed the highest toughness. This is thought to be caused by an interaction of the incident ions with the material such as ion implantation. Best et al. [26] also used different specimen geometries and different notching Ga^+ ion currents to evaluate effect of Ga+ ion on the toughness of CrN thin films. Their results showed that the microcantilever with a Ga+ fabricated notch has higher toughness values than the micropillar without notch, and that the higher the ion current, the higher the measured toughness value.

Additionally, it should be noted here that, although the load-deflection curves reveal that the individual γ lamella shows a good ductility, we did not use the elastic-plastic fracture mechanics, e.g. the J-integral, to evaluate the fracture toughness. This is because we found that the plasticity depends on the position of the notch with respect to γ lamella interface (Fig. 4).

3.2 Deformation and fracture

A TEM foil was cut along the longitudinal direction of the microcantilever with a notch depth of ~ 350 nm. The BF-STEM images are illustrated in Figure 6, showing that the substructure consists of a high density of dislocations and twins which generated in the γ lamella with the notch and its neighbour lamellae. Those dislocations are invisible using 002 reflection (Fig. 6c), which means that they are ordinary dislocations with Burgers vectors of b=$\frac{1}{2}$<110]. This is consistent with the generation of only ordinary dislocations in γ-TiAl alloys with low Al content. Since the density of dislocations is too high, the analysis of Burgers vectors is very difficult. Meanwhile, twinning plays an important role in the fracture of γ-TiAl alloys because crack commonly originates from not only twin-twin interaction and the interaction of twin with the interfaces [27-29], but also twin intersection with grain/colony boundaries [30, 31]. In this study, thus we studied the twinning in the γ lamella. Figure 6 shows that multiple twin systems were activated. One type of twin generated at the top region which is subjected to tension while two types of twins at the bottom region which was subjected to compression. Figure 6c clearly shows that most twins at the top generated at the γ/γ interface and propagated across lamella. It is well established that the lamellar interfaces and grain boundaries are the preferential sites for twin initiation [32]. Electron diffraction analysis indicates that the twin at the top is $(\bar{1}\bar{1}1)[\bar{1}\bar{1}\bar{2}]$ type (Fig. 7a). At the bottom of the cantilever, however, $(111)[11\bar{2}]$ twin for '1' and $(1\bar{1}1)[1\bar{1}\bar{2}]$ twin for '2' in Fig. 7b were activated instead $(\bar{1}\bar{1}1)[\bar{1}\bar{1}\bar{2}]$ twin. The feature '3' close to the lamellar interface in Fig. 7b is also confirmed to be $(111)[11\bar{2}]$ twin. However, the diffraction pattern shows that the region around the twin '3' was seriously deformed with serene lattice distortion (i.e. ~ 2.5° rotation along $[1\bar{1}0]$) (Fig. 8). However, such rotation does not seem apparent in the diffraction pattern for the SAD of twin '1' which is presumably of the same type. Thus, the observed rotation in the SAD of twin '3' may be due to the selected area that included a small volume of an order variant orientated γ lamella nearly, which have been reported to have small (a few degrees) misorientation relative to their neighbours [33]. The lattice distortion induced by deformation was also revealed using local misorentation map that is able to be achieved by transmission Kichuchi diffraction (TKD). Fig. 9 shows a local misorientation distribution for the γ lamella with the notch. Local misorientation presents the misorentation between a given point and its nearest neighbours which belongs to the same grain. The average local misorienation is about 0.8° while the misorientation ahead of the notch tip is up to 4°. Unfortunately, the quality of Kichuchi patterns at the bottom right side of the Fig. 9b is too poor to be indexed, which is due to more serious deformation associated with the cantilever geometry (e.g., closer to the bottom apex, smaller cross-sectional area is, thus more deformation.). As the loading direction is well defined in this experiment, it is possible to calculate the Schmid factors of all of the possible twinning systems. Table 2 presents the Schmid factors for 4 possible

deformation twin systems, showing that at the top of the cantilever the observed twinning system correlates well with the system with highest Schmid factors, consistent with observations in the other alloys [34, 35]. This observation indicates that the predominant activation of deformation systems at the top of the cantilever was a response to the global stress state. More twins were found ahead of the notch tip and twins also generated at sides of the notch. These findings suggest that few, if any deformation twins were punched out the notch tip. Rather, the deformation twins appear to have formed ahead of the notch tip in response to the stress field ahead of the notch. However, at the bottom of the cantilever $(\bar{1}\bar{1}1)[\bar{1}\bar{1}\bar{2}]$ twin with the highest Schmid factor for the global stress was not activated while $(1\bar{1}1)[1\bar{1}\bar{2}]$ and $(111)[11\bar{2}]$ twins with lower Schmid factors generated, which is most likely a response to local stresses probably related to the geometry of the cantilever. For instance, when the cantilever is deflected to a certain displacement, its bottom (especially close to the bottom apex) is not subjected to a simple compression (along the longitudinal direction of the cantilever) but complex stresses.

Amongst those twins observed, nevertheless, the $(\bar{1}\bar{1}1)[\bar{1}\bar{1}\bar{2}]$ twinning generated ahead of the crack (notch) tip, plays a key role in fracture behaviours such as the crack initiation and propagation. The activation of $(\bar{1}\bar{1}1)[\bar{1}\bar{1}\bar{2}]$ twin leads to a twin shear magnitude of $1/\sqrt{2}$ [36] in the $a/6[\bar{1}\bar{1}\bar{2}]$ direction (schematically arrowed on the $(2\bar{1}\bar{1})$ plane in Fig. 6a), thus pushing the γ interface to the built-in end of the microcantilever (arrowed in Fig. 10, and as seen in Fig. 6d). When the strain induced by the $(\bar{1}\bar{1}1)[\bar{1}\bar{1}\bar{2}]$ twin could not be accommodated at the γ interface, that will lead to the formation of microcrack at the γ interface (arrowed in Fig. 10). Additionally, the twin shear on the plane of $(\bar{1}\bar{1}1)$ is able to promote initiation of microcrack on the plane. These two factors may lead to the formation of microcracks on $(\bar{1}\bar{1}1)$ plane and at the γ interface ((111) here). Indeed, cleavage failure features were observed, as seen in Fig. 11a. In the fatigue test of this alloy, the initiation of crack on twin plane, the formation of crack via twin-twin interaction, and the crack initiation on the γ interface by intersection of twin with the interface have been reported earlier [29].

The contribution of $(\bar{1}\bar{1}1)[\bar{1}\bar{1}\bar{2}]$ deformation twin to the plastic strain in the deflection direction of the cantilever (i.e., $[01\bar{1}]$) can be calculated by the following formula:

$$\varepsilon_t = \frac{T \cdot \gamma_t \cdot \sin(\phi)}{w}$$

where ε_t is the plastic strain induced by deformation twin, T is the total twin thickness measured in TEM, γ_t is the twin shear strain equal to $1/\sqrt{2}$, ϕ is the angle between the loading axis (i.e. the horizontal direction of the long axis of the cantilevers) and the active twinning direction, and w is the height of the cantilever measured in SEM before deflection. The formation of those $(\bar{1}\bar{1}1)[\bar{1}\bar{1}\bar{2}]$ twins (Fig. 6) brings about ~ 3% strain in the deflection

direction while ~ 6% strain component perpendicular to the lamellar interface, which inevitably produces a strongly local stress field. This local stress could promote the generation of dislocations and further twinning (e.g. longitudinal twin, parallel to the interface (111) here). Consequently, the local stress is released.

After deformation structure was revealed, we could explain clearly variation in the load with deflection. With increase in the deflection, the load increases linearly and the local stress at the notch tip also rises. When the shear stress ahead of the notch tip is larger than the critical resolved shear stress of $(\bar{1}\bar{1}1)[\bar{1}\bar{1}\bar{2}]$ twin, it will lead to the activation of $(\bar{1}\bar{1}1)[\bar{1}\bar{1}\bar{2}]$ twin (Fig. 3). Then the twin generation results in local stress relaxation, thus dropping the load. Consequently, the serrated load-displacement curve was observed (Fig. 2). Those large load drops (Fig. 2) are associated with motion of twins to the surfaces of the cantilever (Fig. 3). Further deflection produces larger stress field ahead of the notch tip, thus promoting further generation and propagation of twin/slip away from the notch tip. Once twin/slip meet the lamellar interfaces, their movements are impeded somewhat, thus needing a higher stress to keep their motions. Meanwhile, twin-twin interaction, dislocation-dislocation interaction and twin-dislocation interaction will also lead to a high work-hardening. The role of lamellar interfaces in both yield and fracture strength in lamellar TiAl alloy has been described using Hall-Petch –type relationships [37, 38]. If the notch is close to the lamellar interface, it means that slip length of twinning ahead of the notch tip is twice of that in the case of the notch in the middle of the lamella, thus reducing the role of interface. Therefore, a low work-hardening was observed (Fig. 4). As a shearing either along the lamellar interface induced by twinning (i.e. the Mode II component) or perpendicular to the interfaces due to twinning (i.e. the Mode I loading component) is larger than a certain level, the microcantilever fails along the lamellar interface, as seen in Fig. 11b.

4. Conclusions:

The stress intensity factor and fracture behaviour of γ lamella have been investigated using the notched microcantilever test. The deformation microstructure has been examined via TEM. The following conclusions could be made.

1. The notched microcantilever test is a reliable method to evaluate fracture behaviour of individual γ lamella. The fracture stress intensity factor for γ along (111) plane in Ti4522 alloy is 3.1±0.2 MPa $m^{-1/2}$.
2. The activation of $(\bar{1}\bar{1}1)[\bar{1}\bar{1}\bar{2}]$ twin ahead of the notch (crack) tip, governs fracture behaviours such as the crack initiation site and propagation path.
3. The yield point is attributed to the formation of $(\bar{1}\bar{1}1)[\bar{1}\bar{1}\bar{2}]$ twin, does not depend on the positon of the notch with respect to the lamella interface.

4. The work-hardening results from the interaction of twin/slip with lamellar interface.

Acknowledgement

Dr Chu would like to acknowledge the financial support from the Program for Guangdong Introducing Innovative and Enterpreneurial Teams (No. 2016ZT06G025) and Guangdong Natural Science Foundation (No. 2017B030306014), China.

References

1. Y.W. Kim, *Microstructural evolution and mechanical properties of a forged gamma titanium aluminide alloy*, Acta Metall. Mater., 40 (1992), pp.1121-1134.
2. W.J. Porter, M.D. Uchic, R. John, and N.B. Barns, *Compression property determination of a gamma titanium aluminide alloy using micro-specimens*, Script Mater., 61 (2009), pp.678-681.
3. D. Hu and M.H. Loretto, *Slip transfer between lamellae in fully lamellar TiAl alloys*, Intermetallics, 7 (1999), pp.1299-1306.
4. A.J. Palomares-García, M.T. Pérez-Prado, J.M. Molina-Aldareguia, *Effect of lamellar orientation on the strength and operating deformation mechanisms of fully lamellar TiAl alloys determined by micropillar compression*, Acta Mater. 123 (2017), pp.102–114.
5. M. Rester, F. Fischer, C. Kirchlechner, T. Schmoelzer, H. Clemens, G. Dehm, *Deformation mechanisms in micro-sized PST TiAl compression samples: Experiment and model*, Acta Mater. 59 (2011), pp.3410–3421.
6. A.J. Palomares-García, M.T. Pérez-Prado, J.M. Molina-Aldareguia, *Slip transfer across γ-TiAl lamellae in tension*, Mater. & Des., 146 (2018), pp.81-95.
7. T.E.J. Edwards, F. Di. Gioacchino, G. Mohanty, J. Wehrs, J. Michler, W.J. Clegg, *Longitudinal twinning in a TiAl alloy at high temperature by in situ microcompression*, Acta Mater. 148 (2018), pp.202–215.
8. T.E.J. Edwards, F.D. Gioacchino, R.M. Moreno, W.J. Clegg, *Deformation of lamellar TiAl alloys by longitudinal twinning*, Scr. Mater., 118 (2016), pp.46-50.
9. F. Iqbal, J. Ast, M. Göken, and K. Durst, *In situ micro-cantilever tests to study fracture properties of NiAl single crystals*, Acta Mater., 60 (2012), pp.1193-1200.
10. H. Chan, S.G. Roberts, J. Gong, *Micro-scale fracture experiments on zirconium hydrides and phase boundaries*, J. Nuclear Mater., 475 (2016), pp.105-112.
11. Yun. Deng, and Afrooz Barnoush, *Hydrogen embrittlement revealed via novel in situ fracture experiments using notched micro-cantilever specimens*, Acta Mater., 142 (2018), pp. 236-247.

12. T.P. Halford, K. Takashima, Y. Higo, and P. Bowen, *Fracture tests of microsized TiAl specimens*, Fatigue Fract. Eng. Mater. Struct., 28 (2005), pp. 695-701.
13. B.P. Bewlay, S. Nag, A. Suzuki, and M.J. Weimer, *TiAl alloys in commercial aircraft engines*, Mater. High Temp. 33 (2016), pp. 549-559.
14. D. Di Miao and S.G. Roberts, *Measuring fracture toughness of coating using focused-ion-beam-machined microbeams*, J. Mater. Res. 20 (2005), pp. 299-302.
15. K. Matoy, H. Schönherr, T. Detzel, T. Schöberl. R. Pippan, C. Motz, and G. Dehm, *A comparative micro-cantilever study of the mechanical behaviour of silicon based passivation films*, Thin solid films, 518 (2009), pp. 247-256.
16. S. Wurster, C. Motz, and R. Pipan, *Characterization of the fracture toughness of micro-sized tungsten single crystal notched specimens*, Philos. Mag., 92 (2012), pp. 1803-1825.
17. R. Ding, J.C. Gong, A.J. Wilkinson, and I.P. Jones, *Transmission electron microscopy of deformed Ti-6Al-4V micro-cantilevers*, Philos. Mag., 92 (2012), pp. 3290-3314.
18. R. Ding, J.C. Gong, A.J. Wilkinson, and I.P. Jones, *<c+a> dislocations in deformed Ti-6Al-4V micro-cantilevers*, Acta Mater., 76 (2014), pp. 127-134.
19. K.S. Chan and Y.W. Kim, *Effects of lamellar spacing and colony size on the fracture resistance of a fully-lamellar TiAl alloy*, Acta Metall. Mater., 43 (1995), pp. 439–451.
20. K.S. Chan and D. S. Shih, *Fatigue and fracture behaviour of a fine-grained lamellar TiAl alloy*, Metall. Mater. Trans. A, 28 (1997), pp. 79–90.
21. T. Nakano, T. Kawanaka, H.Y. Yasuda, and Y. Umakoshi, *Effect of lamellar structure on fracture behaviour of TiAl polysynthetically twinned crystals*, Mater. Sci. & Eng. A, 194 (1995), pp. 43-51.
22. F. Iqbal, *Fracture Mechanisms of γ–TiAl Alloys Investigated by In-situ Experiments in a Scanning Electron and Atomic Force Microscope*, Ph.D. diss., Friedrich-Alexander-Universität Erlangen-Nürnberg (FAU), 2012.
23. M.H. Yoo, J. Zou, and C.L. Fu, *Mechanistic modelling of deformation and fracture behaviour in TiAl and Ti_3Al*, Mater. Sci. & Eng. A, 192-193 (1995), pp. 14-23.
24. A.S. Booth and S.G. Roberts, *The brittle-ductile transition in γ-TiAl single crystals*, Acta Mater., 45 (1997), pp. 1045-1053.
25. J.P. Best, J. Zechner, I. Shorubalko, J.V. Oboňa, J. Wehrs, M. Morstein, and J. Michler, *A comparison of three different notching ions for small-scale fracture toughness measurement*, Scr. Mater., 112 (2016), pp. 71-74.
26. J.P. Best, J. Zechner, J.M. Wheeler, R. Schoeppner, M. Morstein, and J. Michler, *Small-scale fracture toughness of ceramic thin films: the effects of specimen geometry, ion beam notching and high temperature on chromium nitride toughness evaluation*, Phil. Mag., 96 (2016), pp. 3552-3569.
27. F. Appel, J. D.H. Paul, and M. Oehring, *Gamma Titanium Aluminide Alloys: Science and Technology*, Wiley-Vch Verlag GmbH & Co. kGaA, Weinheim, 2011.

28. Y.H. Lu, Y.G. Zhang, L.J. Qiano, Y.B. Wang, C.Q. Chen, and W.Y. Chu, I*n-situ TEM study of fracture mechanisms of polysynthetically twinned (PST) crystals of TiAl alloys*, Mater. Sci. & Eng. A, 289 (2000), pp. 91-98.
29. R. Ding, H. Li, D. Hu, N. Martin, M. Dixon, and P. Bowen, *Features of fracture surface in a fully lamellar TiAl-base alloy*, Intermetallics, 58 (2015), pp. 36-42.
30. B.A. Simkin, B.C. Ng, M.A. Crimp, and T.R. Bieler, *Crack opening due to deformation twin shear at grain boundaries in near γ-TiAl*, Intemetallics, 15 (2007), pp. 55-60.
31. T.E.J. Edwards, F.D. Gioacchino, R.M. Moreno, and W.J. Clegg, *The interaction of borides and longitudinal twinning in polycrystalline TiAl alloys*, Acta Mater., 140 (2017), pp. 305-316.
32. M.H.Yoo and C.L.Fu, *Physical constants, deformation twinning, and microcracking of titanium aluminides*, Metall. Mater. Trans. A, 29 (1998), pp. 49-63.
33. T.E.J. Edwards, F.D. Gioacchino, and W.J. Clegg, *An experimental study of the polycrystalline plasticity of lamellar titanium aluminide*, Int. J. Plast., 118 (2019), pp. 291-319.
34. B.C. Ng, B.A. Simkin, M.A. Crimp, and T.R. Bieler, *The role of mechanical twinning on microcrack nucleation and crack propagation in a near γ-TiAl alloy*, Intermetallics, 12 (2004), pp. 1317-1323.
35. J. Luster and M.A. Morris, *Compatibility of deformation in two-phase Ti-Al alloys: Dependence on microstructure and orientation relationships*, Metall. Mater Trans A, 26 (1995), pp. 1745-1756.
36. T. Ezaz, H. Sehitoglu, and H.J. Maier, *Energetics of (114) twinning in B2 NiTi under coupled shear and shuffle*, Acta Mater., 60 (2012), pp. 339-348.
37. T. Nakano, A. Yokoyama, and Y. Umakoshi, *Effect of Nb addition on the plastic behavior of TiAl crystals containing oriented lamellae*, Scr. Metall. Mater., 27 (1992), pp. 1253-1258.
38. V.K. Vasudevan, S.A. Court, P. Kurath, and H.L. Fraser, *Effect of grain size and temperature on the yield stress of the intermetallic compound TiAl*, Scr. Metall. Mater., 23 (1989), pp. 467-469.

Table 1 Notch depth and stress intensity factor (K_I) results for tested cantilevers

Specimen #	Notch depth (a), μm	K_I (MPa $m^{-0.5}$)	Comments
1	0.21	2.68	Notch/centre of γ
2	0.21	2.58	Notch/centre of γ
3	0.30	3.13	Notch/centre of γ
4	0.30	3.27	Notch/centre of γ
5	0.31	3.01	Notch/centre of γ
6	0.35	3.02	Notch/centre of γ
7	0.35	3.22	Notch close to interface
8	0.45	3.34	Notch/centre of γ
9	0.60	3.14	Notch/centre of γ
10	0.60	3.17	Notch close to interface
11	0.60	3.35	Notch/centre of γ
12	0.75	2.98	Notch/centre of γ

Table 2 Schmid factors (SF) for various twins at [786] loading axis (the horizontal direction of the long axis of the cantilevers)

Slip plane	Direction	SF	Results (Twin amount / location)
111	$11\bar{2}$	0.08	Minor, at the top; Major, at the bottom
$1\bar{1}1$	$1\bar{1}\bar{2}$	-0.10	All at the bottom
$\bar{1}11$	$\bar{1}1\bar{2}$	-0.12	Not observed
$\bar{1}\bar{1}1$	112	**0.38**	All at top

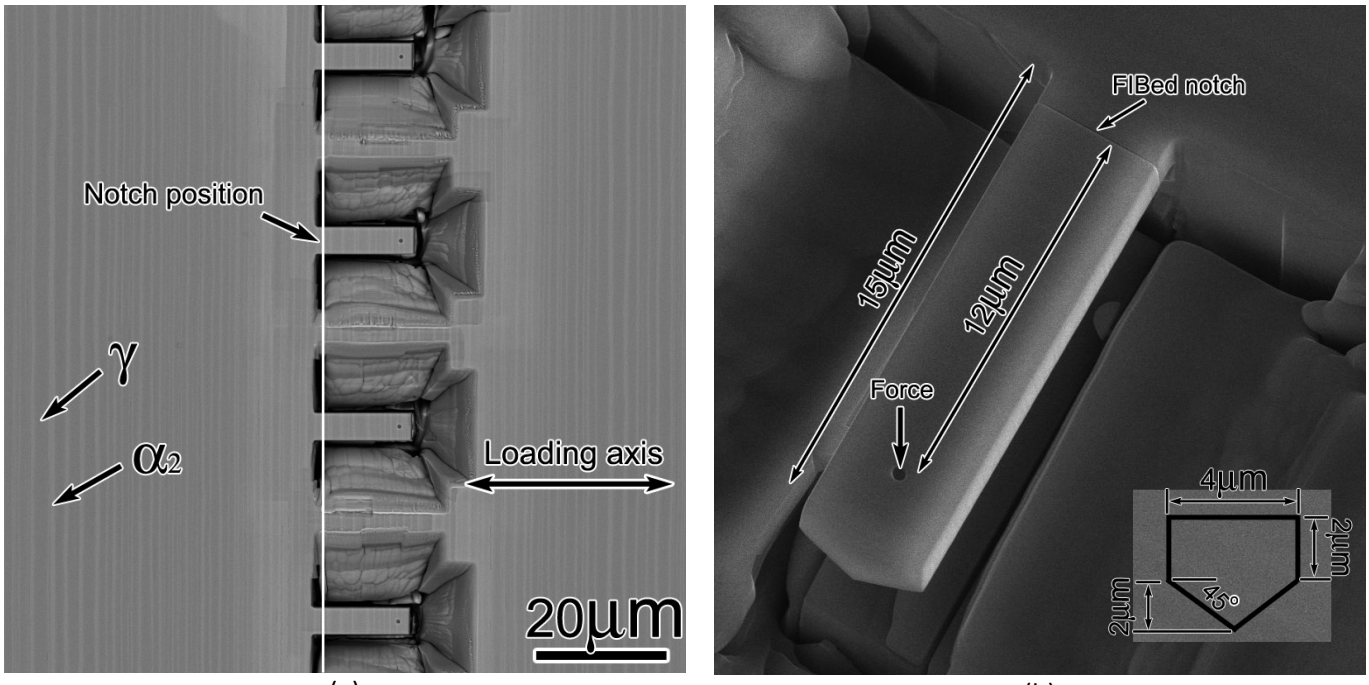

(a) (b)

Figure 1 (a) The notch for each microcantilever milled in the same γ lamella, (b) dimensions of a representative tested microcantilever.

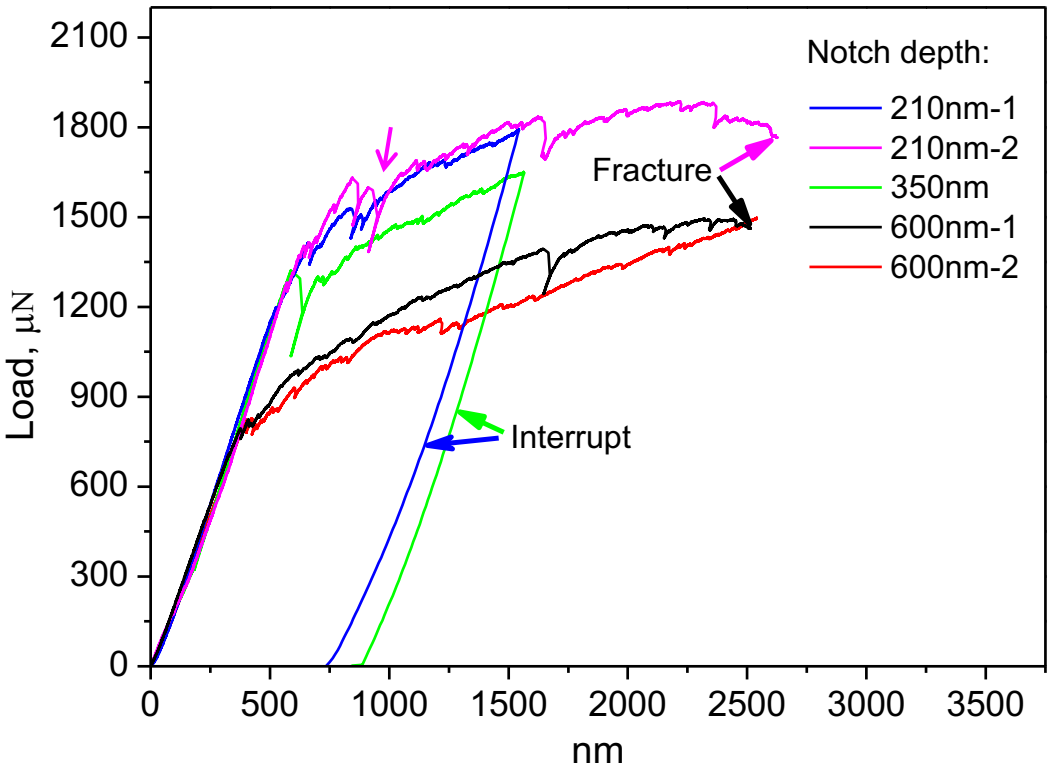

Figure 2 Load-deflection curves of the microcantilevers with the different notch depth.

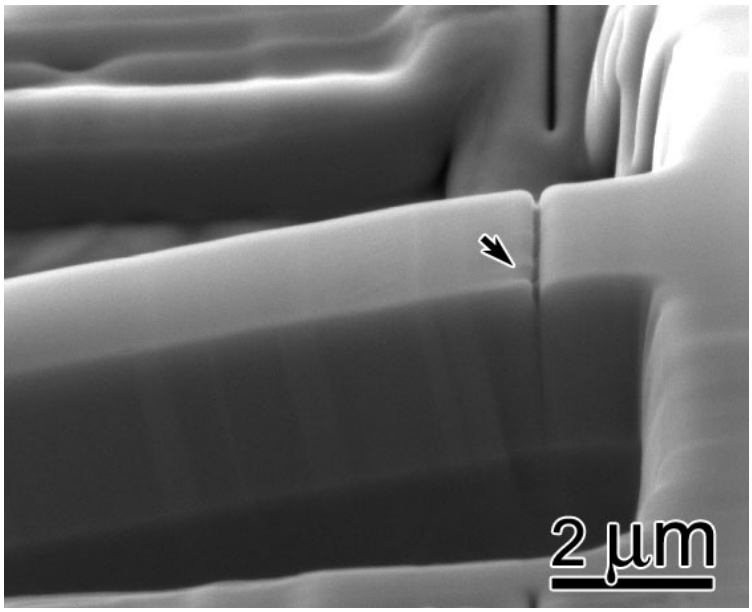

Figure 3 SEM image taken from the microcantilever with 210 nm notch depth after the load drop (arrowed in Fig. 2), showing that the formation of deformation trace is responsible for the load drop.

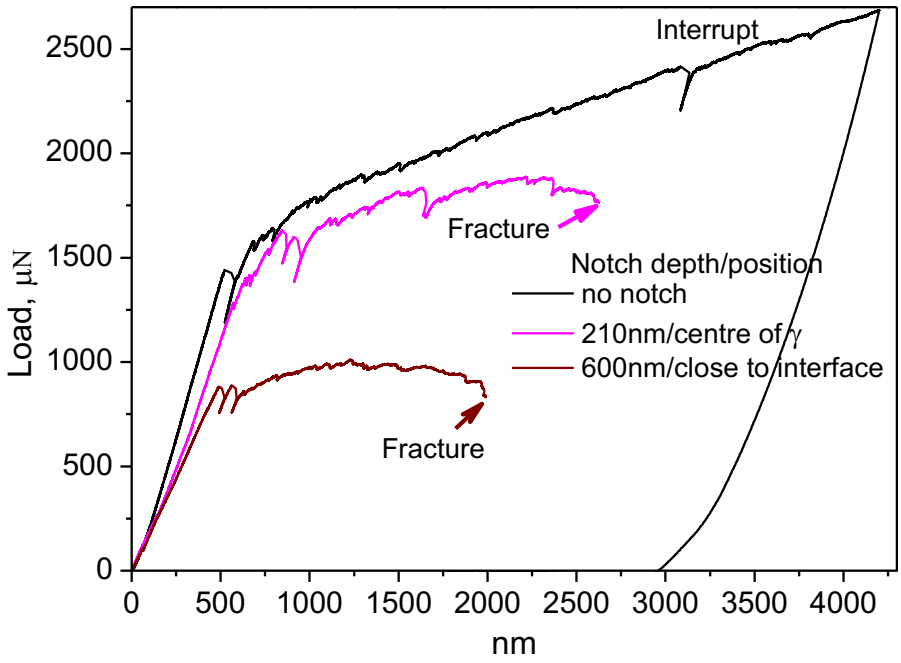

Figure 4 Load-deflection curves of the microcantilevers without notch and with the notches but different positions, revealing that the microcantilever with the notch very close to γ/γ interface shows a lower work-hardening and early failure.

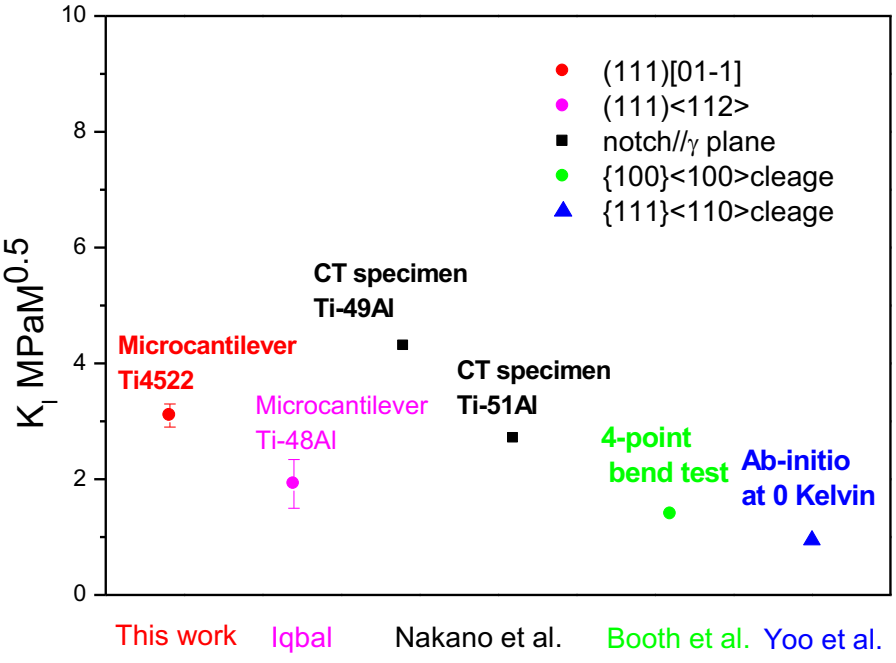

Figure 5 Initiation fracture toughnesses from this study and literature.

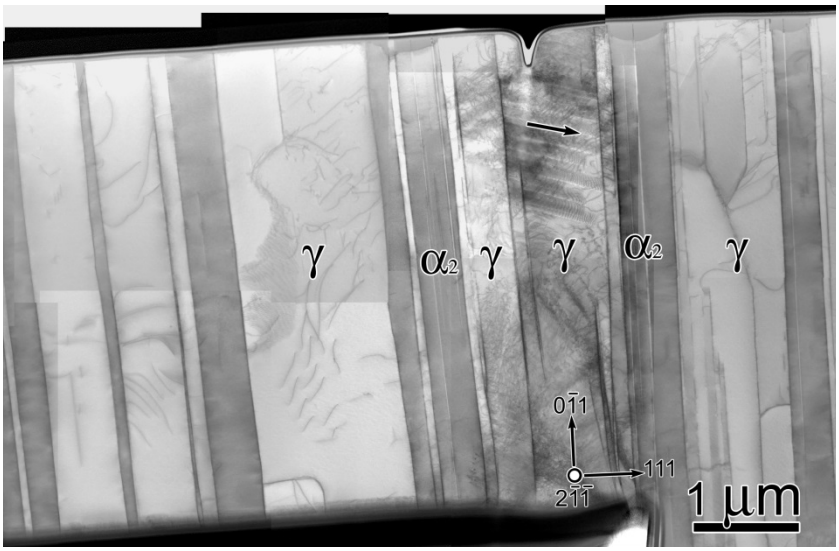

(a)

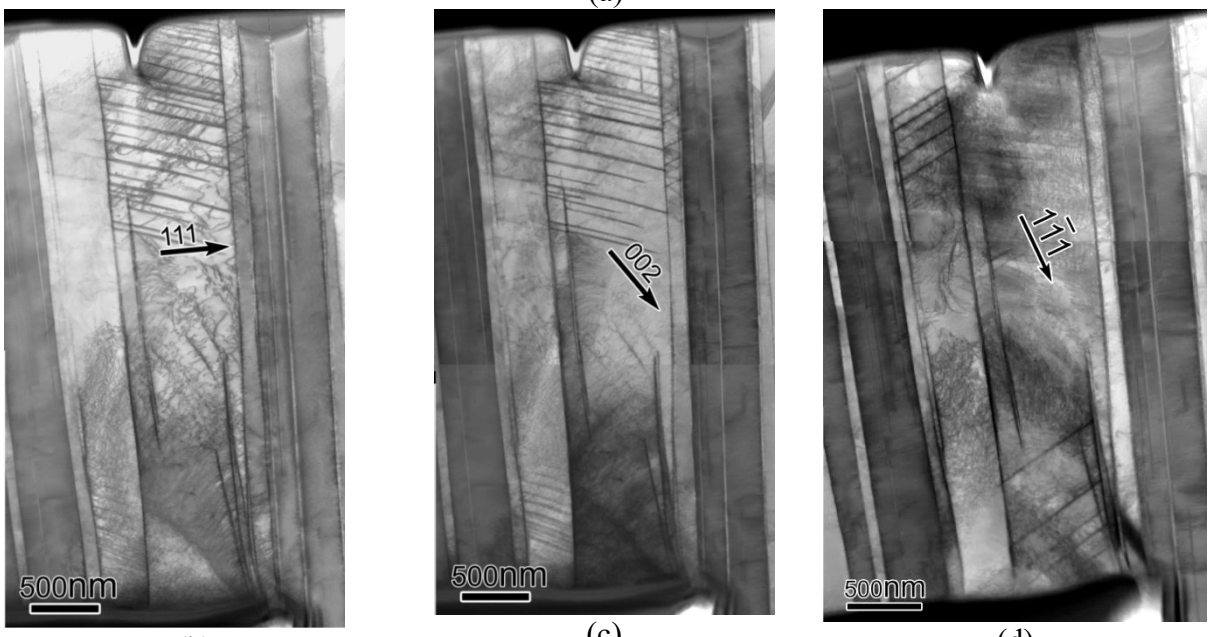

(b) (c) (d)

Figure 6 (a) BF-STEM image from the microcantilever with a notch depth of 350 nm at beam direction (b.d.) of ~ [2$\bar{1}\bar{1}$], (b, c, d) higher magnification images of (a) recorded using different reflections: (b) g = 111 at b.d. of [1$\bar{1}$0], (c) g = 002 at b.d. of [1$\bar{1}$0], and (d) g = 1$\bar{1}$1 at b.d. of [10$\bar{1}$].

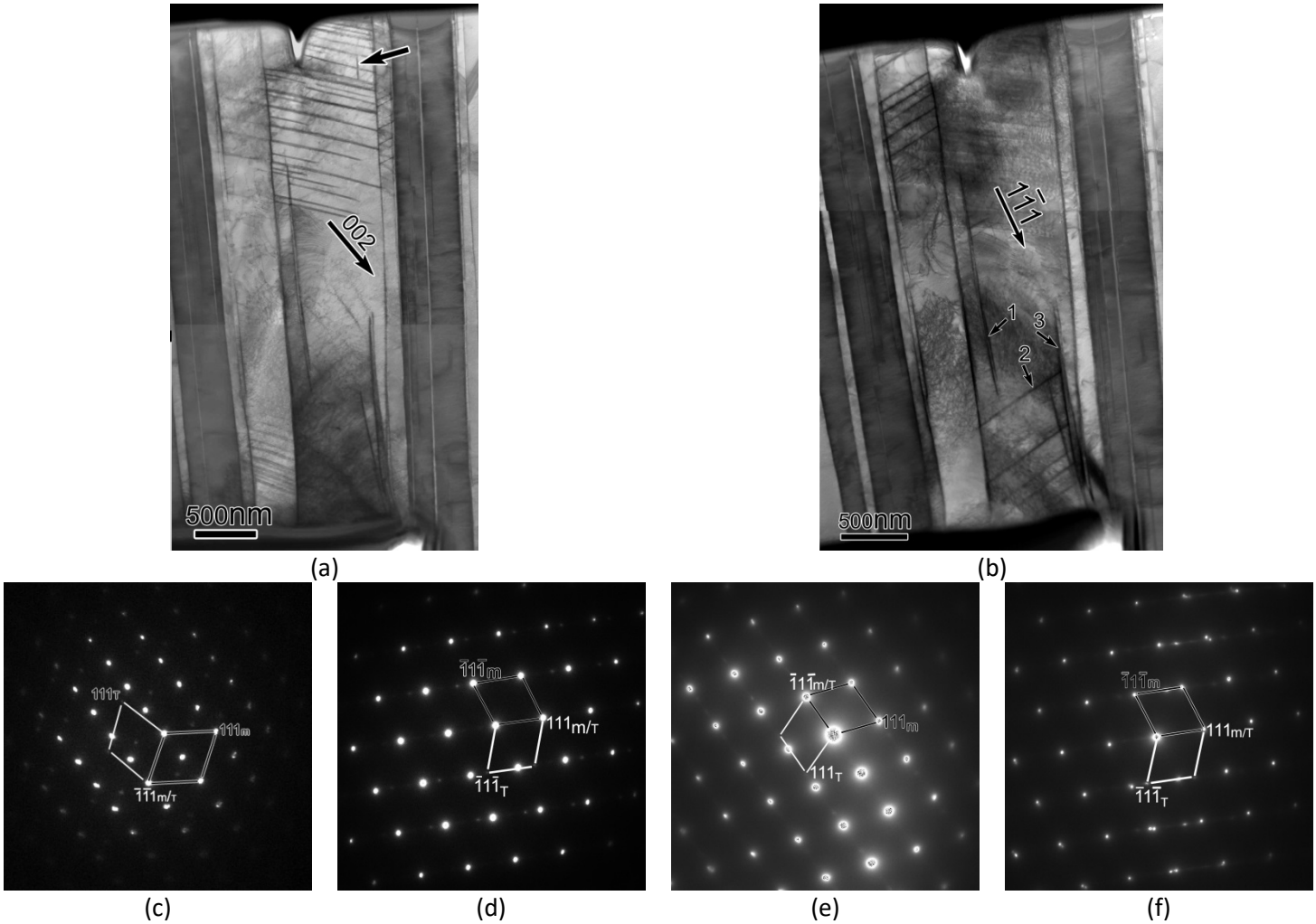

Figure 7 (a and b) BF-STEM images taken from the microcantilever with a notch depth of 350 nm using different reflections, showing twin systems, (c) a selected area diffraction pattern (SAD) from the matrix and twin in the upper of Fig. 7a, (d, e and f) the SADs from '1', '2' and '3' in Fig. 7b, respectively.

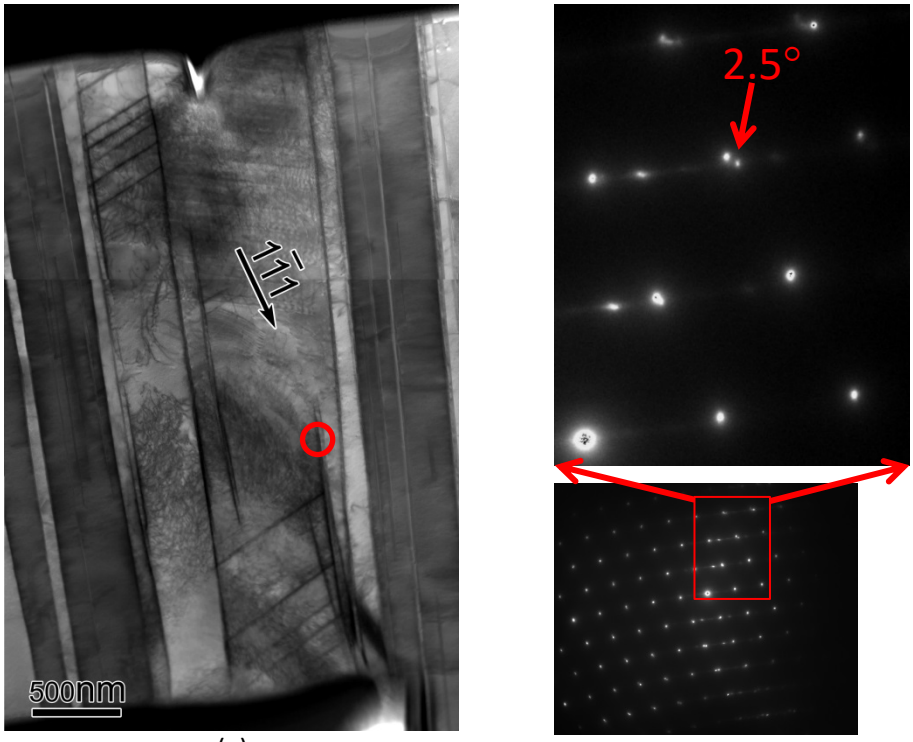

(a) (b)

Figure 8 (a) BF-STM image showing the circled area for diffraction pattern, (b) diffraction pattern along [1$\bar{1}$0] zone axis showing lattice rotated ~ 2.5° along [1$\bar{1}$0] (b).

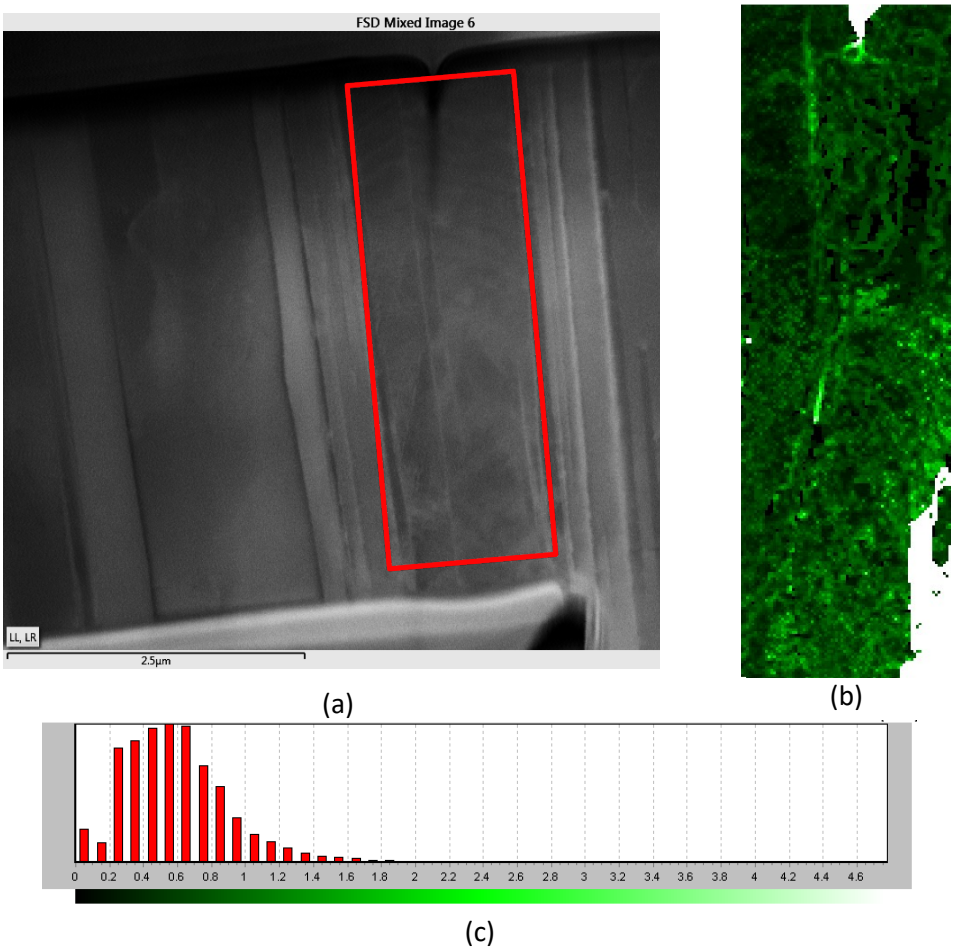

(a) (b)

(c)

Figure 9 (a) SEM image of the TEM sample from the bended microcantilever with a notch depth of 350 nm showing the marked region for transmission Kichuchi diffraction, (b) local misorientation map and (c) local misorientation distribution.

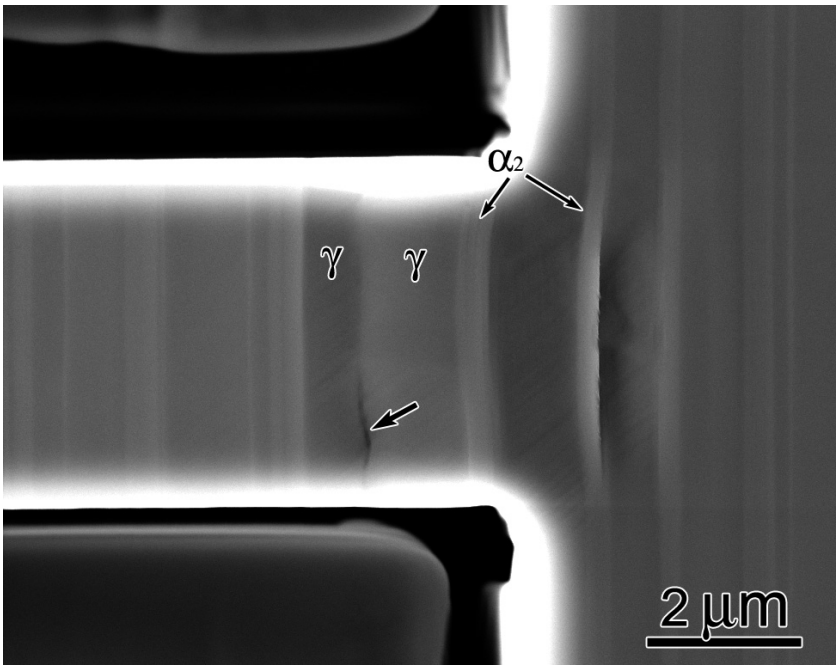

Figure 10 SEM image of a 4.2 μm deflection microcantilever without notch, showing that the portion of the γ/γ interface (arrowed) was bent while its convex surface faces to the built-in side of the microcantilever and that the interfacial microcrack (arrowed) was visible.

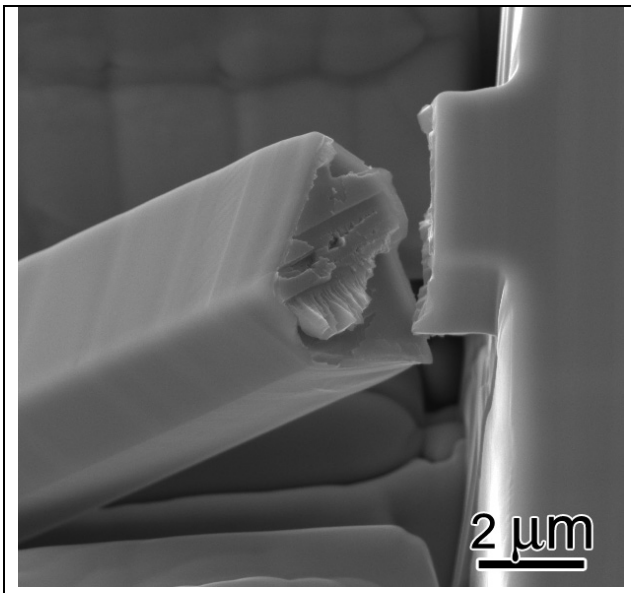

(a)

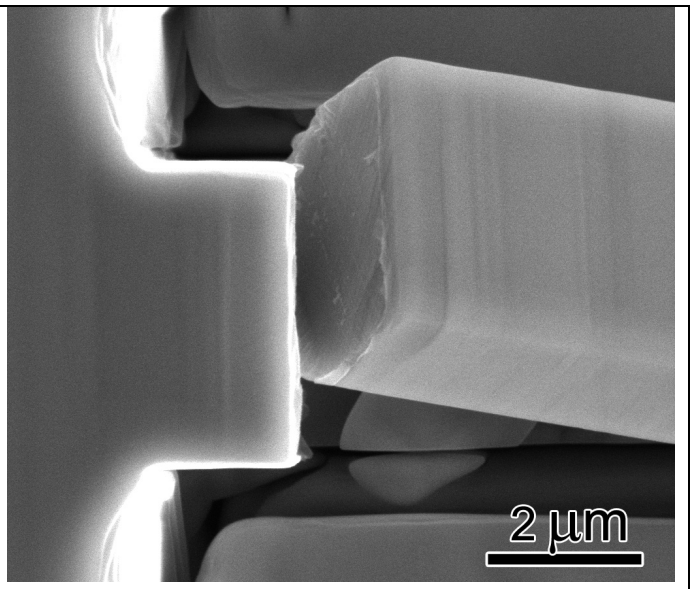

(b)

Figure 11 (a) Fracture surface of a microcantilever with the notch in the middle of the γ lamella, showing that the crack initially propagated along twin boundaries and then deflected to the lamella interface, (b) fractograpy of a microcantilever with the notch close to the γ lamellar interface, exhibiting that the cantilever failed along the lamellar interface.